

Supporting Information

An Ultra-High Mass-Loading Transition Metal Phosphide Electrocatalyst for Efficient Water Splitting and Ultra-Durable Zinc-Air Batteries

Navid Khodayar,^a Abolhassan Noori,^a Mohammad S. Rahmanifar,^b Masumeh Moloudi,^a Nasim Hassani,^c Mehdi Neek-Amal,^{d,e} Maher F. El-Kady,^f Nahla B. Mohamed,^{f,g} Xinhui Xia,^{h,i} Yongqi Zhang,^j Richard B. Kaner^{f,k,*} and Mir F. Mousavi^{a,*}

^a Department of Chemistry, Faculty of Basic Sciences, Tarbiat Modares University, Tehran 14117-13116, Iran. E-mail: mousavim@modares.ac.ir

^b Faculty of Basic Sciences, Shahed University, Tehran 3319118-651, Iran.

^c Department of Chemistry, Razi University, Kermanshah 67149, Iran.

^d Department of Physics, Shahid Rajaee Teacher Training University, Lavizan, Tehran, P.O. Box: 16875-163, Iran.

^e Department of Physics, University of Antwerp, Groenenborgerlaan 171, B-2020 Antwerp, Belgium.

^f Department of Chemistry and Biochemistry and California NanoSystems Institute, University of California, Los Angeles (UCLA), CA 90095, USA. E-mail: kaner@chem.ucla.edu

^g Chemistry Department, Faculty of Science, Cairo University, Giza, 12613 Egypt.

^h College of Materials Science & Engineering, Zhejiang University of Technology, Hangzhou 310014, China.

ⁱ State Key Laboratory of Silicon Materials, Key Laboratory of Advanced Materials and Applications for Batteries of Zhejiang Province, School of Materials Science & Engineering, Zhejiang University, Hangzhou 310027, China.

^j Institute of Fundamental and Frontier Science, University of Electronic Science and Technology of China, Chengdu 611371, China.

^k Department of Materials Science and Engineering, University of California, Los Angeles (UCLA), CA 90095, USA. E-mail: kaner@chem.ucla.edu

1. DFT Convergence Tests

The convergence tests were performed on several key parameters that can significantly impact the results, including k-point mesh, the energy cutoff, and structural relaxations.

K-point Mesh: We adjusted the density of k-points across the Brillouin zone to achieve convergence relative to the dimensions of the supercell or unit cell. This meticulous step is essential for precisely capturing the nuances of the electronic structure and energy contributions within our computational framework. To ascertain convergence, we plotted the energy against the density of k-points, ranging from 2 to 12. Our analysis revealed that the results stabilized and exhibited convergence when employing a k-point mesh of 6. This optimal density ensured that our calculations accurately captured the intricate electronic behaviors and energy dynamics inherent in the system under study.

The Energy Cutoff: We considered a spectrum of cutoff energies to ascertain the convergence of our calculations. Elevating the cutoff energy facilitates a more precise representation of wavefunctions, a critical consideration for systems characterized by intricate electronic structures. We plotted the energy as a function of the energy cutoff, ranging from 280 to 900 eV. Our comprehensive analysis unveiled a definitive convergence pattern, manifesting stability and consistency in results when employing an energy cutoff of 600 eV. This optimal energy threshold ensured that our calculations faithfully captured the nuanced electronic behaviors and energy contributions inherent in the system.

Structural Relaxations: When relaxing the structures, we adhered to standard maximum change values for energy and force as outlined in the literature. Specifically, we set the maximum allowed variations in energy and force during relaxation at 0.01 meV and 0.01 eV/Å, respectively. These thresholds were enforced to ensure the attainment of energetically stable configurations and reliable convergence to the correct equilibrium geometries.

2. Controlled-Potential vs Controlled-Current Electrosynthesis

In controlled-potential electrosynthesis, the working electrode is maintained at a predefined potential. Depending on the selected potential the specific set of analytes will be oxidized/reduced without affecting the other species in the electrolyte that possess more positive (negative) oxidation (reduction) potentials. On the other hand, all the species for which an oxidation/reduction potential is provided will simultaneously undergo a redox reaction. Composition of the electrosynthesized material can be tailored by the chosen potential. In contrast, in a controlled-current electrosynthesis a constant rate of electron flow is requested. Therefore, when the first species can not satisfy the required current, the electrochemical reaction goes to the second species with a higher redox potential to provide that constant current, and in the same way, the next species enter the electrosynthesis process.¹ Thus, the potential of the working electrode is adjusted to maintain that current over the course of the electrosynthesis process. Considering this study, the standard reduction potential for Ni^{2+}/Ni , Co^{2+}/Co , Mn^{2+}/Mn , and $\text{H}_2\text{PO}_2^-/\text{P}$ are -0.257 , -0.280 , -1.185 , and -0.508 V, respectively. As the reduction potential of Ni^{2+} and Co^{2+} are close to each other, they nearly undergo the electrodeposition process concurrently. However, because of the significantly more negative reduction potential of Mn^{2+} , the manganese content of the NCMP electrocatalyst can be tailored via manipulating the electrosynthesis time and current rate. This is why a controlled-current electrodeposition method was purposefully chosen for the electrosynthesis of the NCMP electrocatalyst.

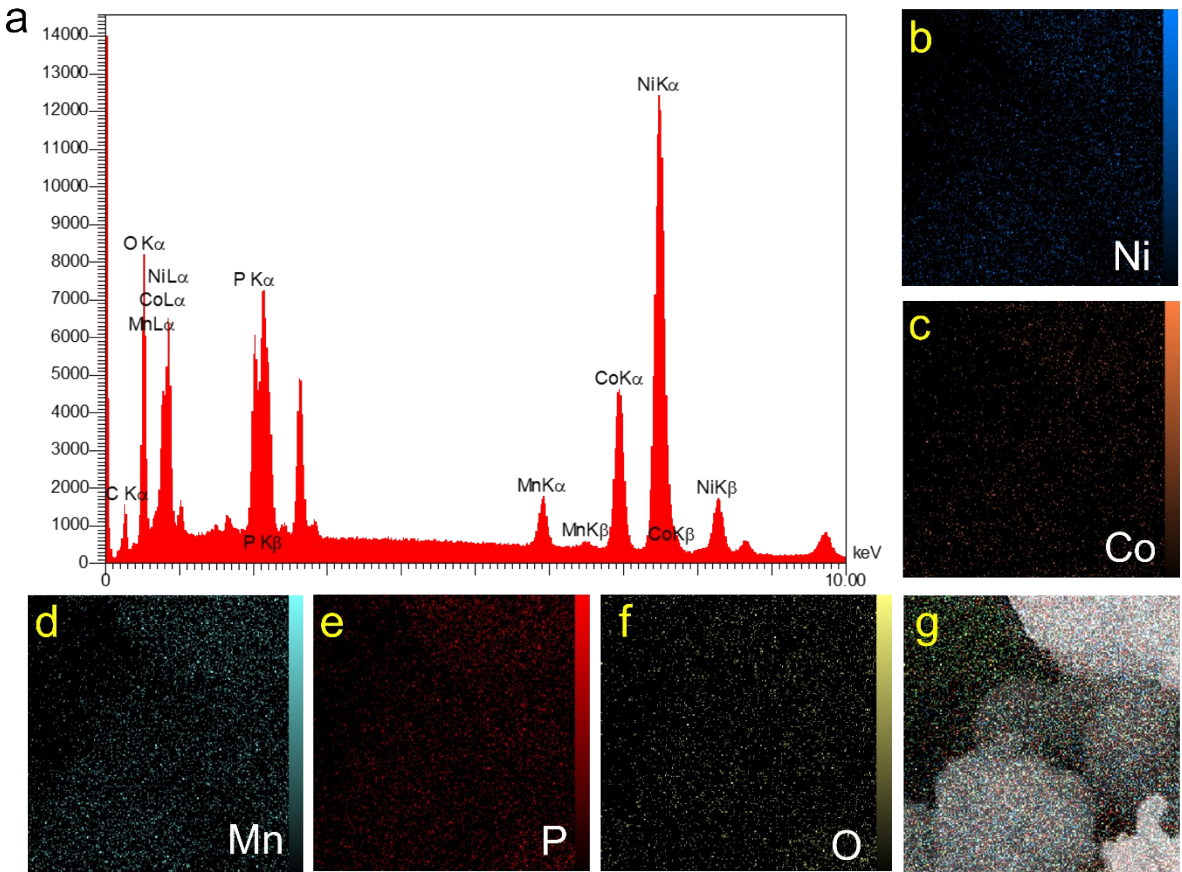


Figure S1. EDX characterization of the NCMP nanostructure. (a) FE-SEM-EDX spectrum and (b-f) elemental mapping of Ni, Co, Mn, P, and O, along with (g) the merged elemental mapping of the NCMP nanostructure.

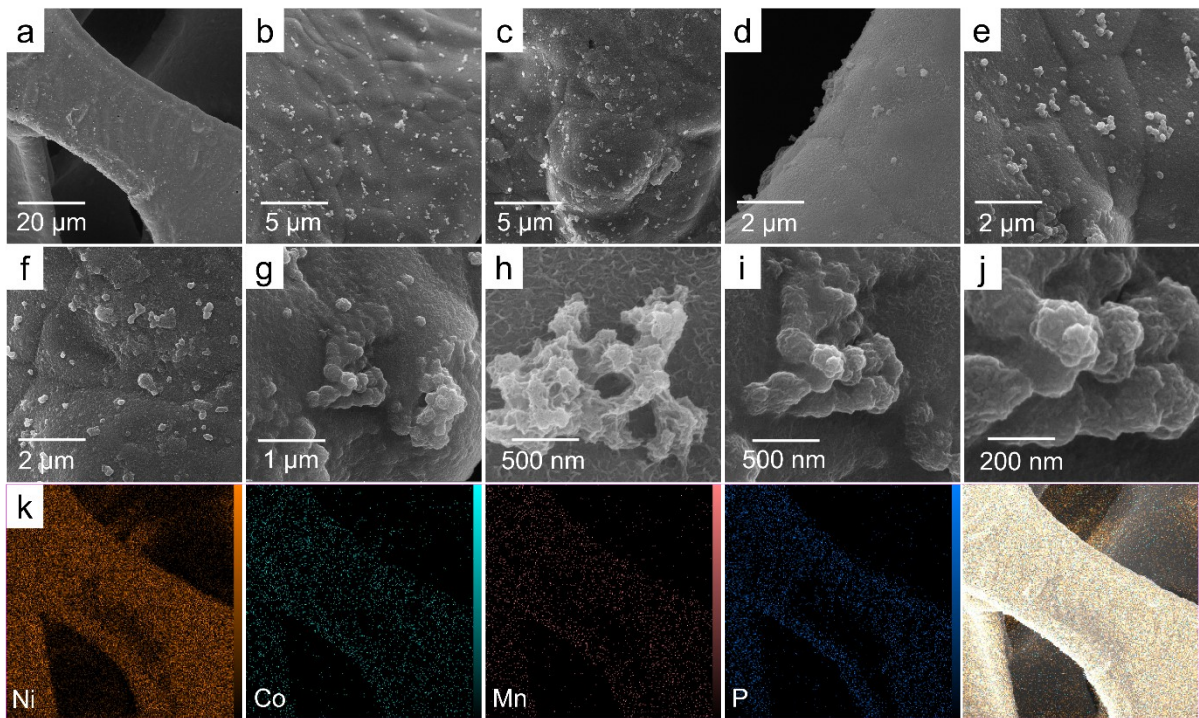
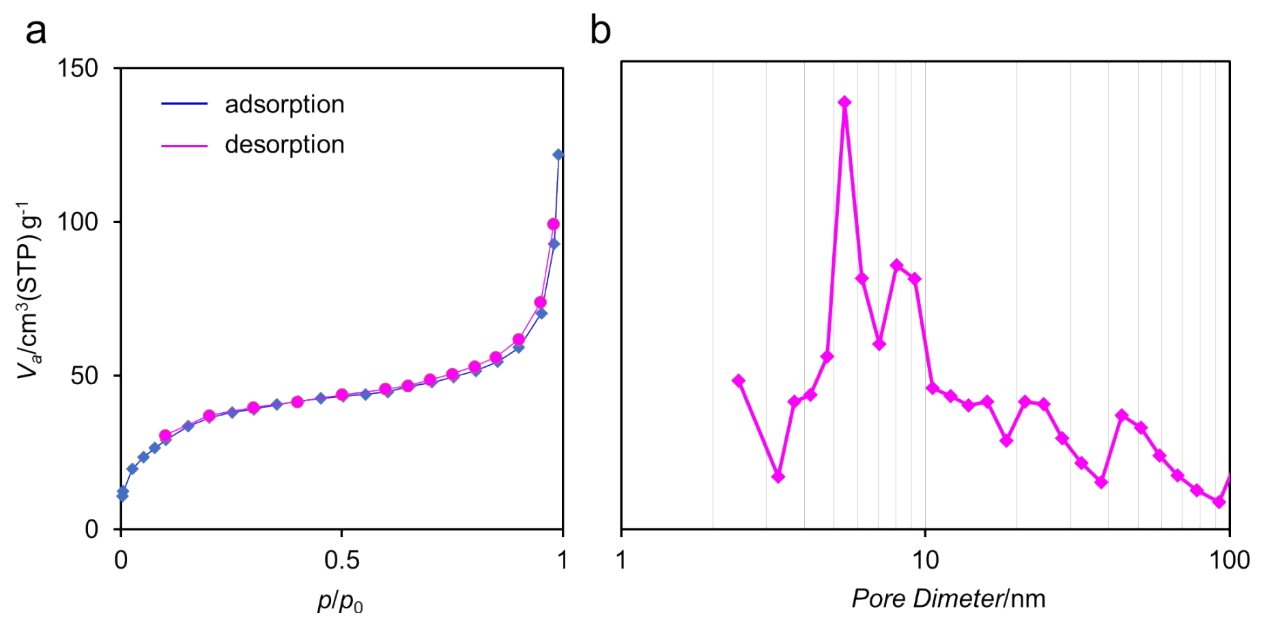


Figure S2. Morphological characterization of the NCMP synthesized without using P123.

(a-j) FE-SEM images of the NCMP catalyst at different magnifications. (k) EDX elemental mapping of Ni, Co, Mn, and P of the NCMP film synthesized in the absence of P123.



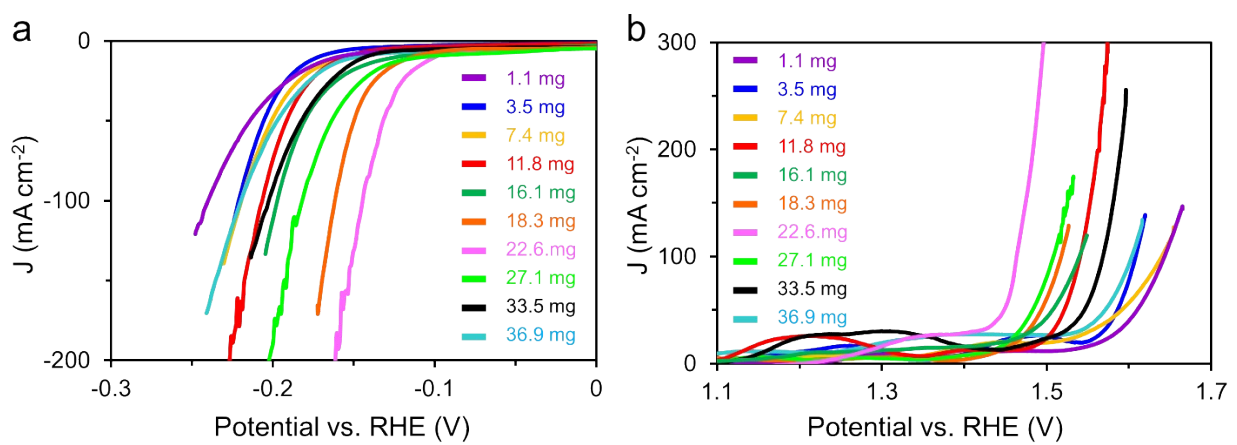


Figure S4. Electrocatalytic activities of the NCMP catalyst with different mass loadings.

(a) The HER and (b) the OER polarization curves of NCMP with different mass loadings from about 1.0 to 37 mg cm⁻², in a 1.0 M KOH electrolyte at a scan rate of 5 mV s⁻¹.

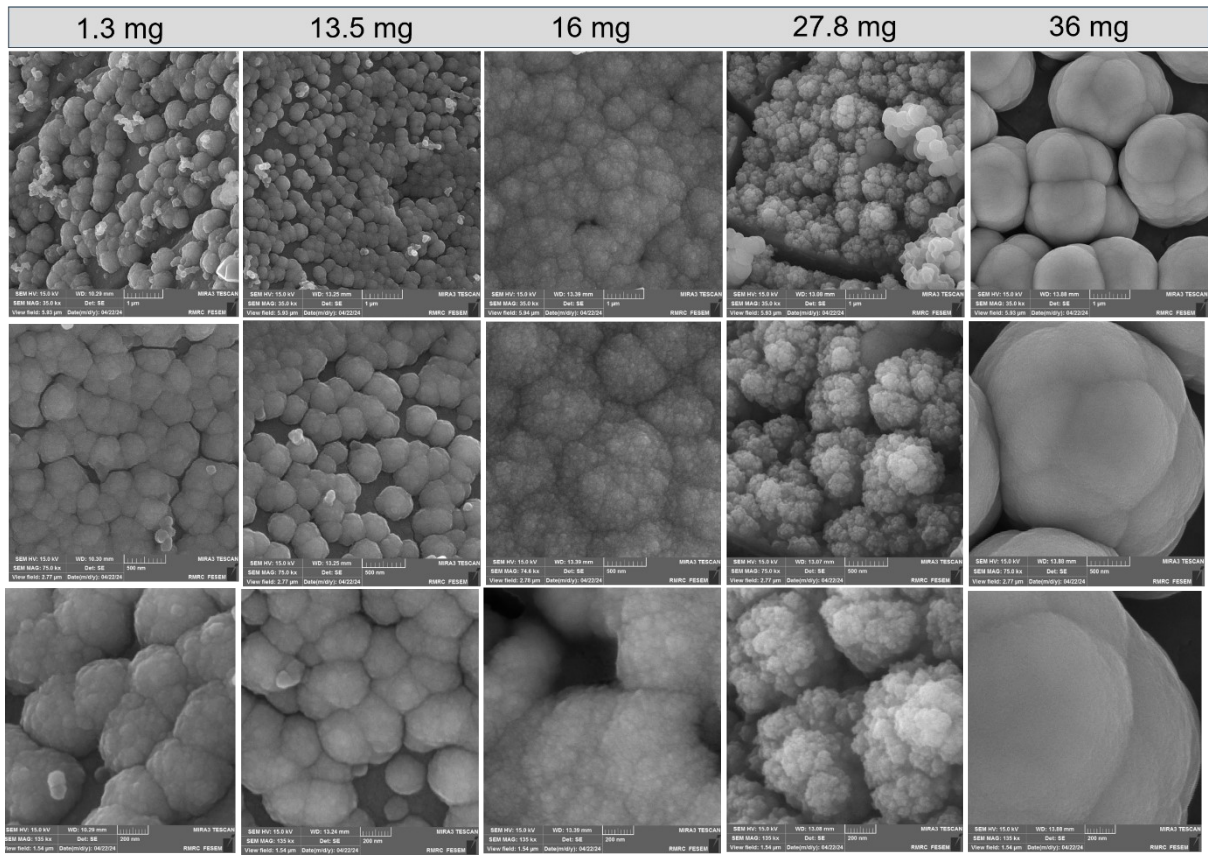


Figure S5. Morphological characterization of the NCMP catalyst with different mass loadings. The FE-SEM images of NCMP with different mass loadings of (1st column) 1.3, (2nd column) 13.5, (3rd column) 16, (4th column) 27.8, and (5th column) 36 mg cm⁻². The scale bars from top to bottom are 1 μm, 500 nm, and 200 nm, respectively.

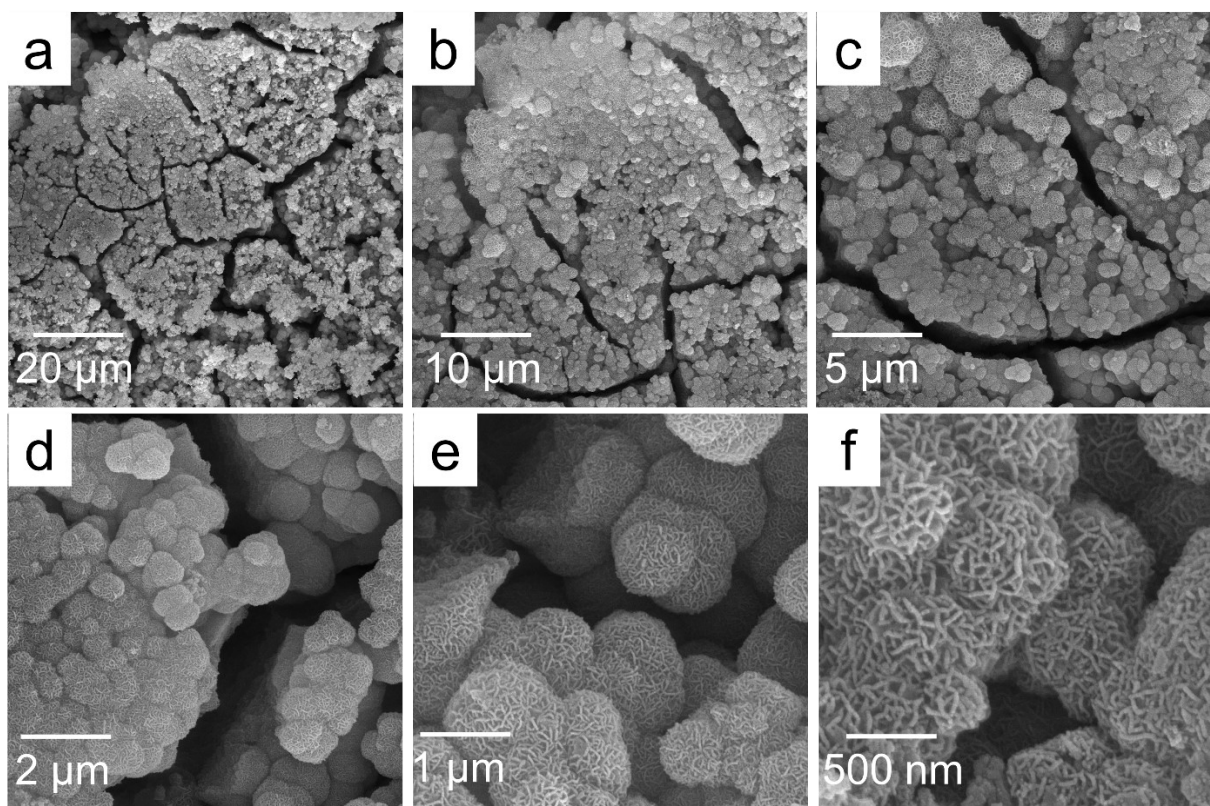


Figure S6. Morphological characterization after long-term HER operation. (a-f) FE-SEM images of NCMP after 120 h of chronoamperometry test for the HER at a rate of -10 mA cm^{-2} in a 1.0 M KOH solution.

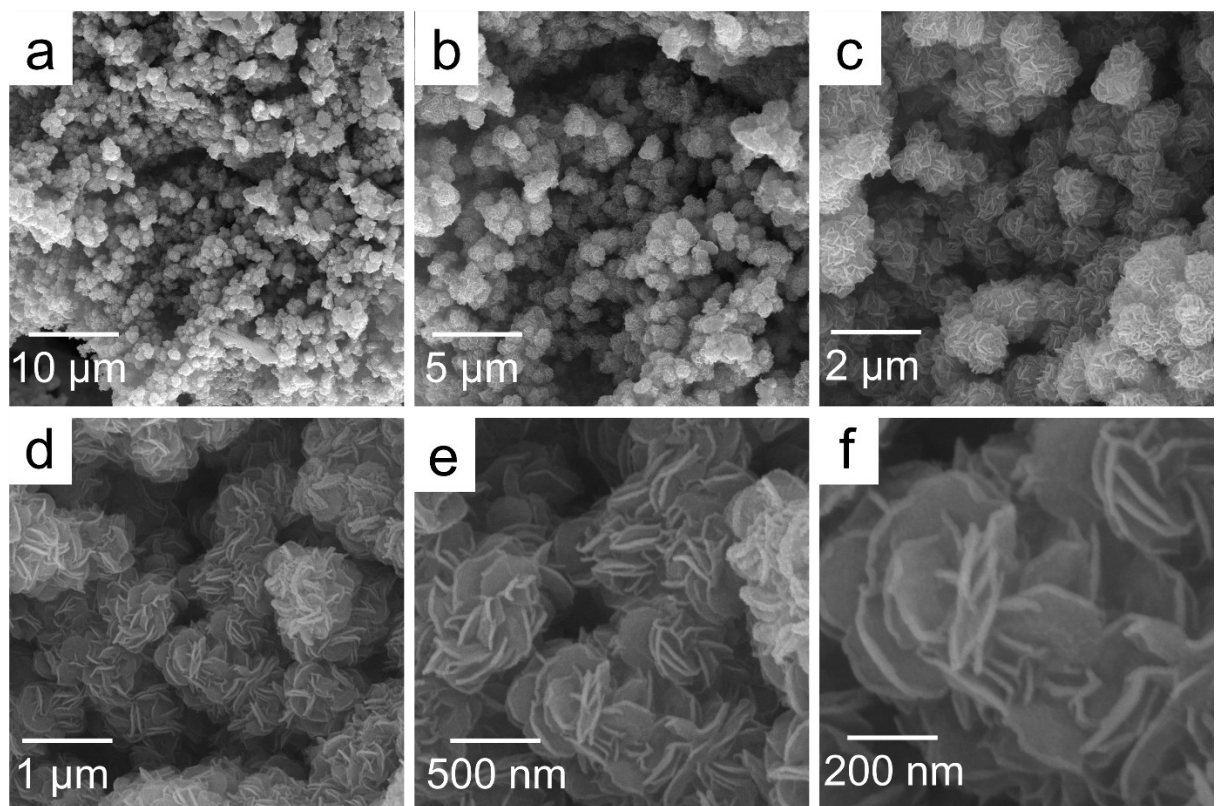


Figure S7. Morphological characterization after long-term OER operation. (a-f) FE-SEM images of NCMP after 120 h of chronoamperometry test for the OER at a rate of 10 mA cm^{-2} in a 1.0 M KOH solution.

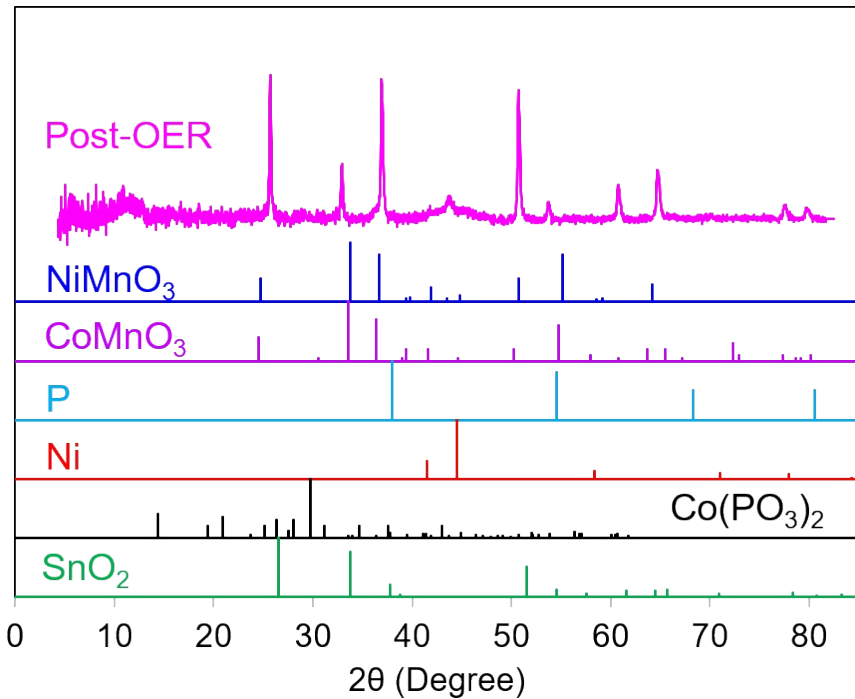


Figure S8. Post-OER XRD characterization. Post-OER surface XRD spectrum of a thin film of the NCMP electrocatalyst after 21 h of OER. Note that, the as-synthesized NCMP electrocatalyst is a powder for which the XRD pattern (**Figure 2f**) is free from parasitic FTO bands. Whereas, for the post-OER surface XRD studies, the electrocatalyst must be electro-synthesized onto a smooth surface (herein a Ni-plated FTO substrate), thus, its bands can be seen in the spectrum.

3. Electrochemical Active Surface Area (ECSA) Measurement

The electrochemical active surface area (ECSA) was estimated by determining the double-layer capacitance (C_{dl} , mF cm^{-2}) from the CV curves obtained at different scan rates within a specific potential range where no Faradaic reaction occurs. The capacitance was then calculated using the following equation:²⁻⁴

$$\Delta J = (2C_{dl}) v \quad (\text{S1})$$

where ΔJ is the double-layer current ($\Delta J = J_{\text{anodic}} - J_{\text{cathodic}}$, mA cm^{-2}) at 1.1 V vs. RHE and v is scan rate (V s^{-1}).

The ECSAs of the catalysts were obtained from Equation S2:

$$ECSA = \frac{C_{dl} \text{ of electrocatalysts } (\text{mF cm}^{-2})}{C_{dl} \text{ of standard (Ni foam, mF cm}^{-2}\text{) per ECSA } (\text{cm}^{-2})} \quad (\text{S2})$$

in which C_{dl} of Ni foam as a standard is 1.7 mF cm^{-2} (much larger than that on an atomically smooth 1.0 cm^2 planar surface, $0.02\text{-}0.06 \text{ mF cm}^{-2}$).

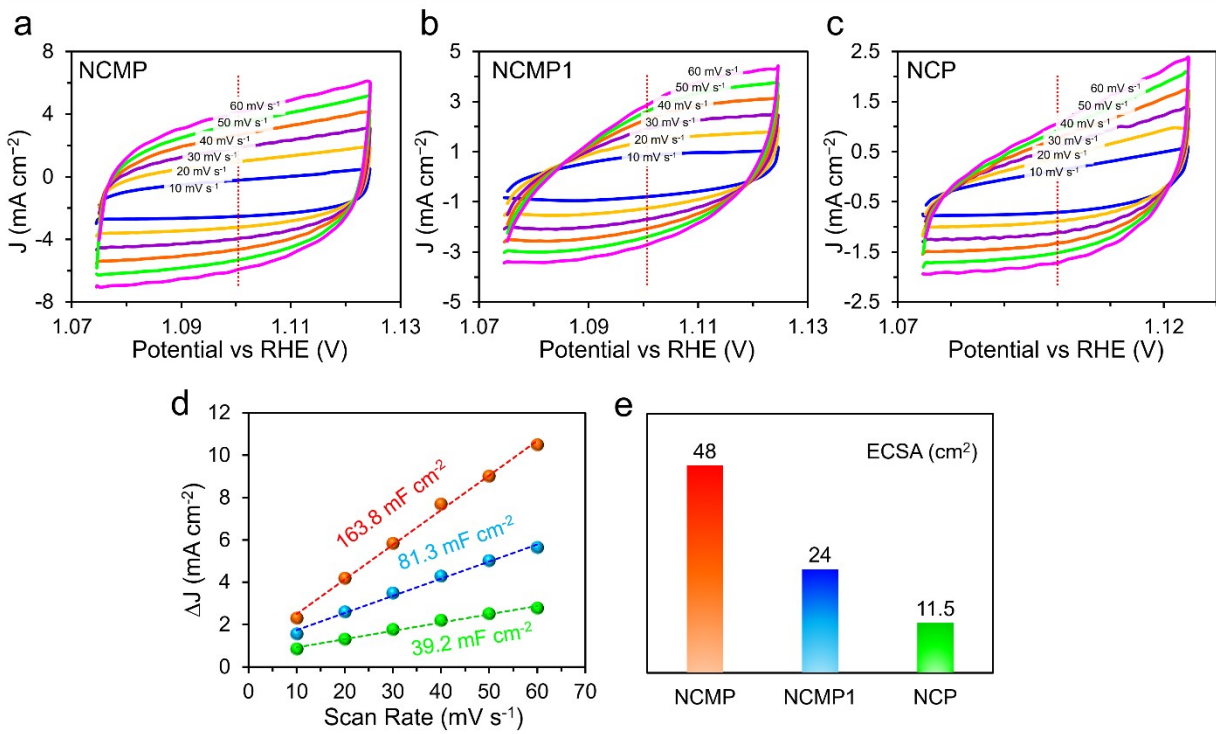


Figure S9. Calculation of ECSA from C_{dl} . CV curves of the (a) NCMP, (b) NCMP1, and (c) NCP at different scan rates from 10-60 mV s⁻¹ in a potential window ranging from 0.05 to 0.1 V vs. Ag/AgCl in an N₂-saturated 1.0 M KOH electrolyte. (d) The plot of capacitive currents ($\Delta J = J_a - J_c$) as a function of scan rate at a potential of 1.1 V vs. RHE from which the C_{dl} can be calculated as half of the slope. (e) The calculated ECSA values from the C_{dl} for the catalysts.

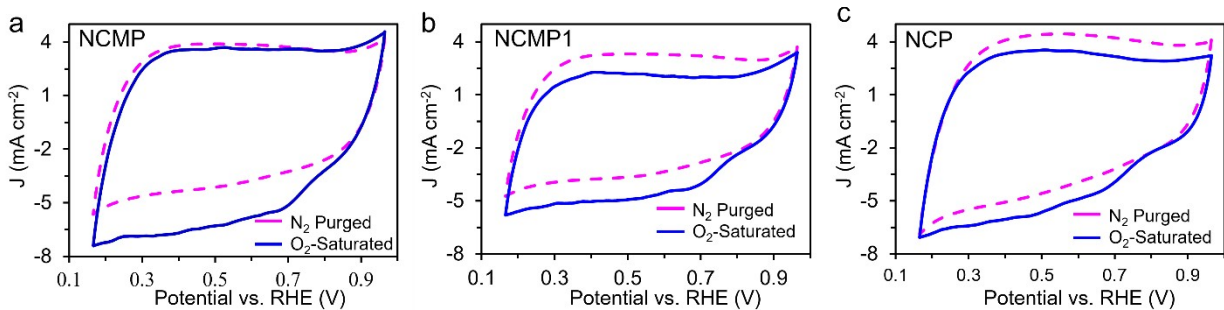


Figure S10. Electrocatalytic study of the m-NCMP nanostructures. The CV curves of the (a) NCMP, (b) NCMP1, and (c) NCP electrocatalysts in O_2 -saturated and N_2 -purged 0.1 M KOH electrolytes at a scan rate of 50 mV s⁻¹.

4. Koutecky-Levich Analysis

The Koutecky-Levich Equation was used to obtain electron transfer numbers and kinetic limiting current densities for ORR at a GC RDE.:^{5,6}

$$\frac{1}{J} = \frac{1}{J_L} + \frac{1}{J_K} = \frac{1}{B\omega^{1/2}} + \frac{1}{J_K} \quad (\text{S3})$$

$$B = 0.62nFC_0D_0^{2/3}\nu^{-1/6} \quad (\text{S4})$$

where J is the measured disk current density, J_L represents the diffusion-limited current density, J_K stands for kinetic-limited current density, ω is the angular velocity of the electrode in rad s⁻¹, n is the overall number of transferred electrons per oxygen molecule in the ORR process, F is the Faraday constant ($F = 96,485 \text{ C mol}^{-1}$), C_0 indicates the bulk concentration of O₂ in a 0.1 M KOH solution ($1.2 \times 10^{-3} \text{ mol cm}^{-3}$), D_0 denotes the oxygen molecule diffusion coefficient in a 0.1 M KOH solution ($1.9 \times 10^{-5} \text{ cm}^2 \text{ s}^{-1}$), and ν is the kinematics viscosity for a 0.1 M KOH electrolyte ($0.01 \text{ cm}^2 \text{ s}^{-1}$).

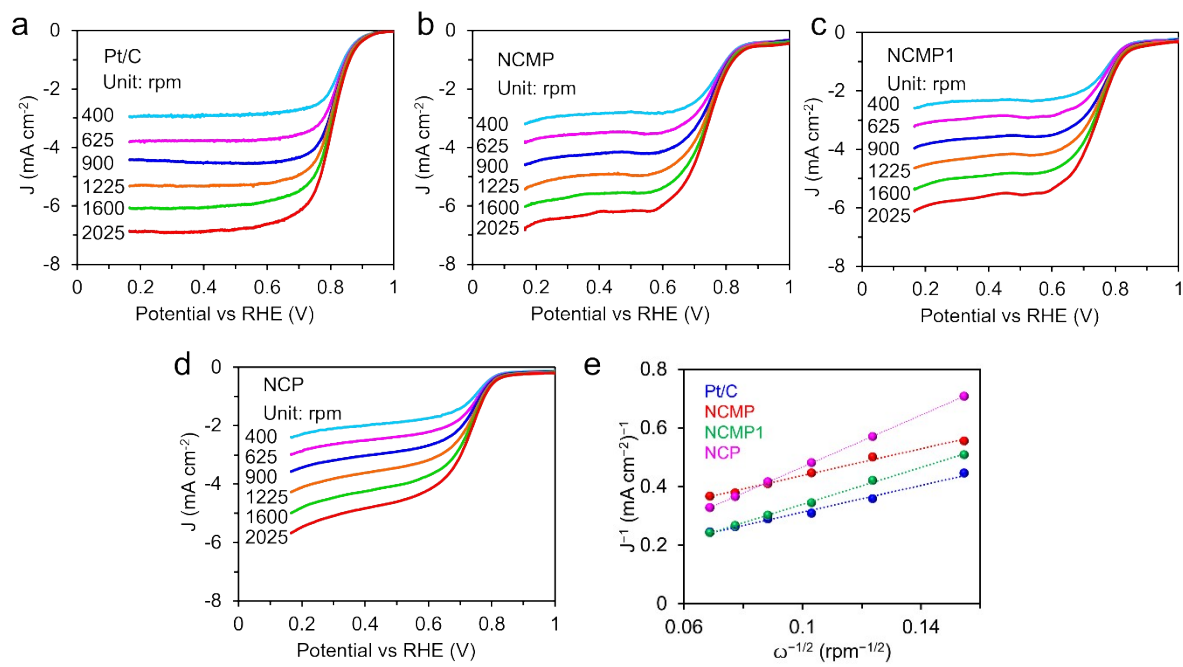


Figure S11. Electrocatalytic ORR activity studies. LSV curves recorded at various rotation speeds on a (a) Pt/C, (b) NCMP, (c) NCMP1, and (d) NCP electrodes in an O_2 -saturated 0.1 M KOH electrolyte at a scan rate of 5 mV s^{-1} . (f) Koutecky–Levich (KL) plots of the electrodes.

5. Characterization of the Rechargeable Zn-air Battery

The specific capacity (C_s , measured in mA h gZn^{-1}) and specific energy (E_s , measured in W h kgZn^{-1}) of the ZABs were obtained by analyzing a GCD profile recorded at a consistent rate of 5 mA cm^{-2} , using the following equations:⁷

$$C_s = \frac{I \times t}{3.6 \times m_{Zn}} \quad (\text{S5})$$

$$E_s = \frac{I \times V \times t}{3.6 \times m_{Zn}} \quad (\text{S6})$$

where I , t , m_{Zn} and V indicate the applied current (A), the discharge time (s), the total weight of the consumed zinc (g), and the corresponding discharge voltage (V), respectively.

6. Theoretical Studies

In an alkaline electrolyte, the OER can be expressed as:

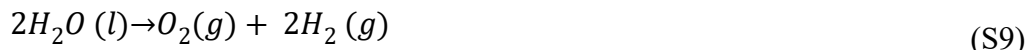


where ΔG_0 is the Gibbs free energy difference for this reaction at $p = 1$ bar and $T = 298.15$ K.

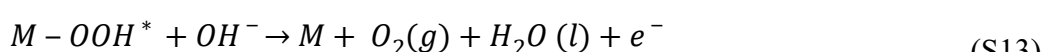
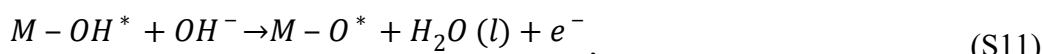
The HER process can be expressed as:



and the overall water splitting reaction is:



The OER reaction contains four elementary steps:



where M refers to the active site on the catalyst and the $M-OH^*$, $M-O^*$, and $M-OOH^*$ denote the adsorbed species on the active site. Under standard conditions, the Gibbs free energy (ΔG) indicates the binding strength between the catalyst and the corresponding intermediates. The typical procedure to calculate ΔG of equations (S10) to (S13) are as follows.

$$\Delta G_1 = E_{OH^*} - E_* - E_{H_2O} + \frac{1}{2} E_{H_2} + (\Delta ZPE - T\Delta S)_1 - eU_{RHE} \quad (\text{S14})$$

$$\Delta G_2 = E_{O^*} - E_{OH^*} + \frac{1}{2} E_{H_2} + (\Delta ZPE - T\Delta S)_2 - eU_{RHE} \quad (S15)$$

$$\Delta G_3 = E_{OOH^*} - E_{O^*} - E_{H_2O} + \frac{1}{2} E_{H_2} + (\Delta ZPE - T\Delta S)_3 - eU_{RHE} \quad (S16)$$

$$\Delta G_4 = E_* - E_{OOH^*} + \left(2E_{H_2O} - \frac{3}{2} E_{H_2}\right) + \Delta G_0 + (\Delta ZPE - T\Delta S)_4 - eU_{RHE} \quad (S17)$$

where ΔZPE and ΔS are the changes in vibrational zero-point energy and entropy from the initial state to the final state, respectively. T is temperature and U_{RHE} is potential of the electrode relative to the RHE. The sum rule is valid for the Gibbs free energies (note that the sum of the changes of the ΔZPE and $T\Delta S$ terms during the reaction cycle equals 0)

$$\Delta G_1 + \Delta G_2 + \Delta G_3 + \Delta G_4 = \Delta G_0 - 4eU_{RHE} \quad (S18)$$

A free energy term contributing to the pH of the electrolyte can be added in Eqs. (S14) to (S17) which can be expressed as:

$$\Delta G_{pH} = pH \times k_B T \ln 10 \quad (S19)$$

And the overpotential for OER (η^{OER}) and ORR (η^{ORR}) reactions can then be calculate as:

$$\eta^{OER} = \frac{1}{en} \max_{n=1,2,3,4} [\Delta G_n] - U_0 \quad (S20)$$

$$\eta^{ORR} = \frac{1}{en} \max_{n=1,2,3,4} [-\Delta G_n] + U_0 \quad (S21)$$

where $U_0 = \Delta G_0 / 4e = 1.23$ V is the equilibrium potential and is independent of pH.

For the HER, the free energy of the steps associated with adsorption of H can be estimated according to:

$$\Delta G_H = \Delta E_H + (\Delta ZPE - T\Delta S_H) - eU_{RHE} \quad (S22)$$

where ΔE_H is the hydrogen chemisorption energy which can be calculated using the following equation:

$$\Delta E_H = E_{H^*} - E_* - \frac{1}{2} E_{H_2} \quad (\text{S23})$$

where E_{H^*} refers to the total energy of complex of the adsorbed hydrogen on the active site of the catalyst.

7. DFT Calculation on the Active Site

The electron localization function (ELF) and charge density difference maps are illustrated in **Figure S12**. A value of 0.950 signifies a fully localized electron, whereas a value of 0.035 indicates a very low charge density. While the ELF of the Mn-P, Co-P, and Ni-P bonds is similar, the charge density difference map reveals subtle distinctions among them. In the trimetallic NCMP system, the high electron density regions are almost situated at the midpoint of the triangle formed by the metal atoms. This suggests partial transition of the nonpolar σ covalent bonds into ionic bonds. The electronegativity differences for the Mn-P, Co-P, and Ni-P bonds are 1.49, 1.16, and 1.13, respectively. The increase in electronegativity difference indicates a shift toward polarity, and the corresponding ELF becomes more localized. Our Hirshfeld charge analysis indicates that the charges of Mn, Co, Ni, and P atoms are approximately $+0.22 |e|$, $+0.04 |e|$, $+0.02 |e|$, and $-0.11 |e|$, respectively. This suggests electron deficiency on the metallic sites (Mn, Co, Ni), and electron excess on P. Considering all this, the active site is likely the trimetallic center, as their bonding characteristics are largely similar to each other and they cooperate synergistically during the electrocatalytic processes.

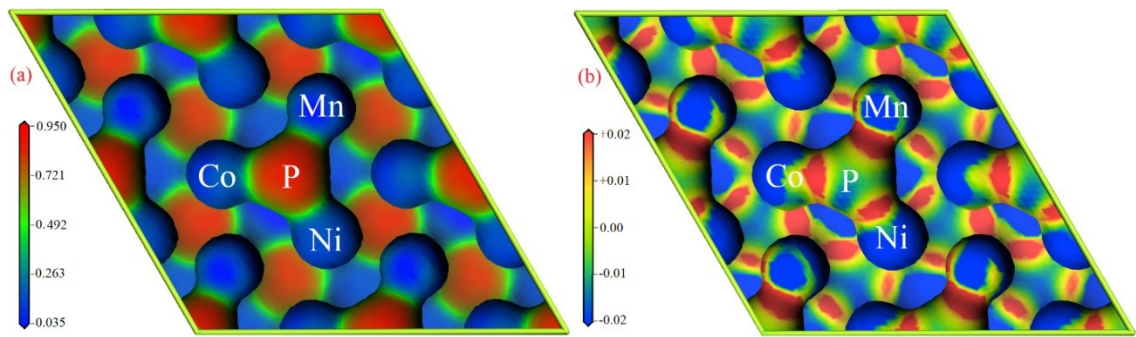


Figure S12. (a) Electron localization function (ELF) and (b) charge density difference maps of the NCMP electrocatalyst.

Table S1: Comparison of the Electrocatalytic HER and OER Activities of the NCMP Catalyst with Other Catalysts Reported in the Literature

Material	Mass loading (mg cm ⁻²)	Electrolyte	η_{HER} (mV)	η_{OER} (mV)	OWS (V)	Ref.
Ni₂P/FeP-FF	2.0	1.0 M KOH	$\eta_{10} = 42$	$\eta_{10} = 217$	1.69	[⁸]
FeP	1.0 M KOH	$\eta_{10} = 218$	$\eta_{10} = 216$	1.68	[⁹]
CoFeP@C	1.0 M KOH	$\eta_{10} = 181$	$\eta_{10} = 262$	1.55	[¹⁰]
CoP-NC@NFP	1.0 M KOH	$\eta_{10} = 162$	$\eta_{10} = 270$	1.57	[¹¹]
			$\eta_{10} = 84$			
CeO₂-NiCoP	2.09	1.0 M KOH	$\eta_{500} = 202$ $\eta_{1000} = 242$	$\eta_{30} = 255$	1.59 (J = 50 mA)	[¹²]
(Cu₃P-Cu₂O/NPC	2.5	1.0 M KOH	$\eta_{10} = 138$	$\eta_{10} = 286$	1.57 (J = 10 mA)	[¹³]
c-CoMP/a-CoM	1.0 M KOH	$\eta_{100} = 191.8$	$\eta_{100} = 333.2$	1.655 (J = 100 mA)	[¹⁴]
Co@CoFe-P	0.3	1.0 M KOH	$\eta_{10} = 83$	$\eta_{10} = 266$	1.49 (J = 10 mA) 1.54 (J = 100 mA)	[¹⁵]
CoP-HS	1.0 M KOH	$\eta_{10} = 116$	$\eta_{10} = 281$	1.67 (J = 50 mA)	[¹⁶]
FeP-350/NF	1.0 M KOH	$\eta_{100} = 413$	$\eta_{100} = 388$	1.54 (J = 10 mA)	[¹⁷]
			$\eta_{10} = 111$	$\eta_{10} = 283$		
CoP₃-Nb₂P/PCC	3.8	1.0 M KOH	$\eta_{500} = 317$ $\eta_{1000} = 375$	$\eta_{100} = 366$ $\eta_{500} = 478$	1.66 (J = 10 mA)	[¹⁸]
CoP/DCS	1.0 M KOH	$\eta_{10} = 88$	$\eta_{10} = 251$	1.49 (J = 10 mA)	[¹⁹]
MnOx/NiFeP/NF	1.0 M KOH	$\eta_{500} = 255$	$\eta_{500} = 296$ $\eta_{1000} = 346$	1.796 (J = 500 mA) 1.828 (J = 1000 mA)	[²⁰]
Co₂P CuP₂/NF	9.82	1.0 M KOH	$\eta_{10} = 93$	$\eta_{10} = 220$	1.77 (J = 500 mA) 2.38 (J = 1000 mA)	[²¹]
CoP-NC@NFP	1.0 M KOH	$\eta_{10} = 162$	$\eta_{10} = 270$	1.57 (J = 10 mA)	[¹¹]
Ni₂P/CoP	1.0 M KOH	$\eta_{10} = 87.8$	[²²]
Co@CoP₂/CF(1:1)	0.5	1.0 M KOH	$\eta_{10} = 55$	$\eta_{10} = 210$	1.54 (J = 10 mA)	[²³]
Ni-CoP-2	0.5 M H ₂ SO ₄	$\eta_{10} = 110$	[²⁴]
		1.0 M KOH	$\eta_{10} = 157$	$\eta_{10} = 306$	1.69 (J = 10 mA)	

F-CDs/CoP	1.0 M KOH	$\eta_{10} = 16$	$\eta_{20} = 161$	1.48 (J = 10 mA)	[²⁵]
MNC-P/NF	0.6	1.0 M KOH	$\eta_{10} = 14$	$\eta_{10} = 289$	1.48 (J = 10 mA)	[²⁶]
Ru-CMOP	1.0 M KOH	$\eta_{100} = 114$	$\eta_{100} = 286$	1.697 (J = 100 mA) 1.828 (J = 500 mA)	[²⁷]
5MT-P	1.0 M KOH	$\eta_{50} = 220$	$\eta_{50} = 226$	1.69 (J = 100 mA)	[²⁸]
Ni₂P@Ti₃C₂Tx	0.5 M H ₂ SO ₄	$\eta_{10} = 123.6$	[²⁹]
CoxP/NC-Mel	1.0 M KOH	$\eta_{50} = 312$	[³⁰]
Cu₃P/Ni₂P@CF	1.0 M KOH	$\eta_{10} = 88.1$	$\eta_{50} = 330$	1.56 (J = 10 mA)	[³¹]
(Fe,Ni)3P/NiCoP	5.5	0.5 M H ₂ SO ₄ 1.0 M PBS 1.0 M KOH	$\eta_{10} = 50.9$ $\eta_{10} = 70.5$ $\eta_{10} = 52.3$	[³²]
S-NiFeP-10	3.0	1.0 M KOH	$\eta_{10} = 56$	$\eta_{10} = 201$	1.5 (J = 10 mA)	[³³]
CoP@CF-900	1.0 M KOH	$\eta_{50} = 190$	$\eta_{50} = 340$	1.89 (J = 200 mA)	[³⁴]
NiCoP-MoS₂-VMo	1.0 M KOH	$\eta_{10} = 67$	[³⁵]
Zn doped CoFeP@NC	1.0 M KOH	$\eta_{10} = 270$ $\eta_{100} = 313$	[³⁶]
CoFeP@C	0.5	1.0 M KOH	$\eta_{10} = 181$	$\eta_{10} = 262$	1.55 (J = 10 mA)	[¹⁰]
Ru-CoP/CC	1.0 M KOH	$\eta_{10} = 45$	[³⁷]
CoP/FeOOH	1.4	Alkaline	$\eta_{10} = 250$	[³⁸]
Co(OH)₂/NiPx	1.0 M KOH	$\eta_{10} = 236$	[³⁹]
CoP/C/Cu	2.0	0.5 M H ₂ SO ₄	$\eta_{100} = 151$	[⁴⁰]
Ni_{2-x}Rh_xP C-NPs	0.28	1.0 M KOH	$\eta_{10} = 82.1$	$\eta_{10} = 273.1$	1.78 (J = 20 mA)	[⁴¹]
Co-P@IC/(Co-Fe)P@CC	1.0 M KOH	$\eta_{10} = 53$	$\eta_{10} = 174$	1.46 (J = 10 mA)	[⁴²]
C@NiCoP	0.5	1.0 M KOH	$\eta_{10} = 46.3$	[⁴³]
CoP₃/Ni₂P	4.0	1.0 M KOH	$\eta_{100} = 167.5$	$\eta_{100} = 291$	1.557 (J = 10 mA)	[⁴⁴]
		0.1 M KOH	$\eta_{100} = 194.1$	$\eta_{100} = 296$	1.595 (J = 10 mA)	
		1.0 M PBS	$\eta_{100} = 181.8$	$\eta_{100} = 314$	1.628 (J = 10 mA)	
Al, Fe-codoped CoP/RGO	0.3	0.5 M H ₂ SO ₄ 1.0 M KOH	$\eta_{10} = 138$ $\eta_{10} = 145$	$\eta_{10} = 312$ $\eta_{10} = 280$	1.66 (J = 10 mA)	[⁴⁵]
CFC@EC	1.0 M KOH	$\eta_{10} = 39$	$\eta_{10} = 222$	1.53 (J = 10 mA)	[⁴⁶]

NiMn-P	1.5	1.0 M KOH	$\eta_{10} = 92$	$\eta_{10} = 190$	1.49 (J = 10 mA)	[47]
CP@NCNT	0.54	1.0 M KOH	$\eta_{10} = 94$	$\eta_{10} = 317$	1.619 (J = 10 mA)	[48]
a-NiHCF	4.9	1.0 M KOH	$\eta_{400} = 280$ $\eta_{800} = 309$	[49]
CLDH/CP/CF	7.4	1.0 M KOH	$\eta_{10} = 111$	$\eta_{10} = 221$	1.575 (J = 10 mA)	[50]
Rh₂P-N/P-CC	2.5	1.0 M KOH	$\eta_{20} = 4$	$\eta_{20} = 274$	1.7 (J = 200 mA)	[51]
			$\eta_{100} = 44$	$\eta_{100} = 349$		
			$\eta_{200} = 71.5$	$\eta_{200} = 388$		
			$\eta_{400} = 115$	$\eta_{400} = 447$		
Ni₂P-Fe₂P	15.0	1.0 M KOH	$\eta_{10} = 128$ $\eta_{100} = 225$	$\eta_{100} = 261$ $\eta_{1000} = 337$	1.682 (J = 100 mA) 1.865 (J = 500 mA)	[52]
W2C/WP@NC	1.0	0.5 M H ₂ SO ₄ 1.0 M KOH	$\eta_{10} = 196.2$ $\eta_{10} = 116.37$	[53]
FeCoP₂@NPPC	0.5 M H ₂ SO ₄	$\eta_{10} = 114$	$\eta_{10} = 236$	1.60 (J = 10 mA) (In 1.0 M KOH)	[54]
		1.0 M KOH	$\eta_{10} = 150$			
CoFe-P/NF-1	1.0 M KOH	$\eta_{100} = 180$	$\eta_{200} = 275$	1.57 (J = 10 mA)	[55]
NiFeP/CC	1.0 M KOH	$\eta_{10} = 129$	$\eta_{200} = 260$	1.57 (J = 10 mA)	[56]
(Ni_xFe_{1-x})₂P@PC/PG	2.4	1.0 M KOH	$\eta_{10} = 66$	$\eta_{50} = 268$	1.45 (J = 10 mA)	[57]
CoP/N, P-doped C	1.0	1.0 M KOH	$\eta_{10} = 103$	$\eta_{30} = 260$	1.54 (J = 10 mA)	[58]
0D@2D Ni₂P@NSG	0.5 M H ₂ SO ₄	$\eta_{10} = 124$	$\eta_{10} = 240$	1.572 (J = 10 mA)	[59]
		1.0 M KOH	$\eta_{10} = 110$			
Ru₁CoP/CDs	0.5 M H ₂ SO ₄	$\eta_{10} = 49$	[60]
		1.0 M KOH	$\eta_{10} = 51$			
CoP@FeCoP/NC YSMPs	1.0	1.0 M KOH	$\eta_{10} = 141$	$\eta_{10} = 238$	1.68 (J = 10 mA)	[61]
Ni₂P-CuP₂	11.25	0.5 M H ₂ SO ₄	$\eta_{10} = 12$ $\eta_{100} = 124$	$\eta_{20} = 140$ $\eta_{50} = 190$	1.45 (J = 10 mA)	[62]
		1.0 M KOH			
NiFeP@NC/Ni₂P	1.0 M KOH	$\eta_{20} = 223$	1.57 (J = 10 mA)	[63]
Ni₃P:FeMo	1.0 M KOH	$\eta_{100} = 103$	$\eta_{100} = 290$	1.48 (J = 10 mA)	[64]
CPN@TC	3.01	1.0 M KOH	$\eta_{10} = 15$	[65]
Fe-Co₂P@Fe-N-C	1.0 M KOH	$\eta_{10} = 77$	$\eta_{10} = 300$	1.58 (J = 10 mA)	[66]
Co-NixPy@Co₃O₄/NF	1.0 M KOH	$\eta_{10} = 72$	$\eta_{10} = 120$	1.47 (J = 20 mA)	[67]
CoP/Mo₂CT_x	Cathode: 1.428	1.0 M KOH	$\eta_{10} = 78$	$\eta_{10} = 260$	1.56 (J = 10 mA)	[68]
	Anode: 0.4					

CoP-NCDs/NF	1.0 M KOH	$\eta_{10} = 103$	$\eta_{10} = 226$	1.55 (J = 10 mA)	[⁶⁹]
Cr-CoP/CP	0.5 M H ₂ SO ₄	$\eta_{10} = 47$	
		1.0 M PBS	$\eta_{10} = 131$	
		1.0 M KOH	$\eta_{10} = 67$	$\eta_{10} = 251$	1.49 (J = 10 mA) 1.73 (J = 100 mA)	[⁷⁰]
Co-Mo-P@NCNS-600	1.0 M KOH	$\eta_{10} = 62$	$\eta_{10} = 270$	1.58 (J = 10 mA)	[⁷¹]
NiCoP-p	2.61	0.5 M H ₂ SO ₄	$\eta_{10} = 53$	
		1.0 M PBS	$\eta_{10} = 92$	$\eta_{10} = 395$	
		1.0 M KOH	$\eta_{10} = 55$	$\eta_{20} = 254$	1.49 (J = 10 mA) 1.85 (J = 500 mA)	[⁷²]
MoP@NC-250	0.75	1.0 M KOH	$\eta_{10} = 96$	[⁷³]
NiCoFeMnCrP	1.0 M KOH	$\eta_{10} = 220$	$\eta_{10} = 270$	1.55 (J = 10 mA)	[⁷⁴]
CP	5.2	1.0 M KOH	$\eta_{10} = 78.4$	$\eta_{10} = 234.2$ $\eta_{120} = 344.6$	1.49 (J = 10 mA)	[⁷⁵]
Co₂P/CoNPC	0.39	1.0 M KOH	$\eta_{10} = 208$	$\eta_{10} = 326$	1.64 (J = 10 mA)	[⁷⁶]
CoFeO@BP	0.4	1.0 M KOH	$\eta_{10} = 88$	$\eta_{10} = 266$	1.584 (J = 10 mA)	[⁷⁷]
CoP@PNC-DoS	0.28	0.1 M KOH	$\eta_{10} = 173$	$\eta_{10} = 316$	1.719 (J = 10 mA)	[⁷⁸]
Fe0.29Co0.71P/NF	4.1	1.0 M KOH	$\eta_{50} = 112$ $\eta_{200} = 116$	$\eta_{50} = 251$ $\eta_{200} = 259$	1.59 (J = 10 mA)	[⁷⁹]
CoP-InNC@CNT	0.35	1.0 M KOH	$\eta_{10} = 159$	$\eta_{10} = 270$	1.58 (J = 10 mA)	[⁸⁰]
CoP NFs	0.265	1.0 M KOH	$\eta_{10} = 136$	$\eta_{10} = 323$	1.65 (J = 10 mA)	[⁸¹]
CoP/Ti₃C₂ MXene	1.0 M KOH	$\eta_{10} = 102$	$\eta_{10} = 280$	1.578 (J = 10 mA)	[⁸²]
Mo-Ni₃S₂/NixPy/NF	3.15	1.0 M KOH	$\eta_{10} = 109$	$\eta_{10} = 238$	1.46 (J = 10 mA)	[⁸³]
(Fe_{0.1}Ni_{0.9})₂P(O)/NF	20.0	1.0 M KOH	$\eta_{10} = 87$	$\eta_{10} = 207$ $\eta_{100} = 240$	1.50 (J = 10 mA)	[⁸⁴]
Ru-MnFeP	1.0 M KOH	$\eta_{10} = 191$	1.47 (J = 10 mA)	
Ru-MnFe				$\eta_{10} = 262$	1.546 (J = 10 mA)	[⁸⁵]
ZnCo ₂ (PO ₄) ₂	0.1 M KOH	$\eta_{10} = 450$	
ZnCoP ₂ O ₇			$\eta_{10} = 460$	[⁸⁶]
Ni₃N-VN/NF	1.0 M KOH	$\eta_{10} = 64$	1.51 (J = 10 mA)	
Ni₂P-VP₂/NF			$\eta_{50} = 306$	1.48 (J = 10 mA) 1.57 (J = 10 mA)	[⁸⁷]
NF@Fe₂-Ni₂P/C	3.9	1.0 M KOH	$\eta_{10} = 39$	$\eta_{10} = 205$	1.57 (J = 10 mA)	[⁸⁸]

FeNiP/PG	2.00	1.0 M KOH	$\eta_{10} = 173$	$\eta_{10} = 229$	1.58 (J = 10 mA)	[⁸⁹]
Cu0.075Co0.0925P/CP	5.00	1.0 M KOH	$\eta_{10} = 70$	$\eta_{10} = 221$	1.55 (J = 10 mA)	[⁹⁰]
ZnS-CoP/CP	3.00	1.0 M KOH	$\eta_{10} = 49$	$\eta_{10} = 233$	1.51 (J = 10 mA)	[⁹¹]
NiP/NiFeP/C	0.168	1.0 M KOH	$\eta_{10} = 138$	$\eta_{10} = 250$	1.53 (J = 10 mA) 1.68 (J = 100 mA)	[⁹²]
Co/CoxMy	0.57	1.0 M KOH	$\eta_{10} = 330$	[⁹³]
Mn _x (PO ₄) _y /NPC	0.5	1.0 M KOH	$\eta_{10} = 370$	[⁹⁴]
Co ₂ P NC	0.2	1.0 M KOH	$\eta_{10} = 62.5$	$\eta_{10} = 280$	1.56 (J = 10 mA)	[⁹⁵]
NiFe LDH@NiCoP/NF	2	1.0 M KOH	$\eta_{10} = 120$	$\eta_{10} = 220$	1.57 (J = 10 mA)	[⁹⁶]
Co ₄ Ni ₁ P NTs	0.19	1.0 M KOH	$\eta_{10} = 129$	$\eta_{10} = 245$	1.59 (J = 10 mA)	[⁹⁷]
(Co _{0.52} Fe _{0.48}) ₂ P	2.5	1.0 M KOH	$\eta_{10} = 79$	$\eta_{10} = 270$	1.53 (J = 10 mA)	[⁹⁸]
CoMnP	0.28	1.0 M KOH	$\eta_{10} = 330$	[⁹⁹]
NCMP	22.6	1.0 M KOH	$\eta_{10} = 100$	$\eta_{50} = 218$	1.53 (J = 10 mA)	This Work

Table S2: Comparison of the Electrocatalytic Activity of the NCMP Catalyst as the Air Cathode of a Zn-Air Battery with Other Catalysts Reported in the Literature

Catalyst	Capacity (mA h g ⁻¹ _{zn}) (At current density, mA cm ⁻²)	Power density (mW cm ⁻²)	Specific energy W h kg ⁻¹ (At current density, mA cm ⁻²)	ΔE _(ORR-OER) (V)	OCV (V)	First round-trip efficiency (%) (At current density, mA cm ⁻²)	Ref.
CoP/CoO@MNC-CNT	724.6 (5 mA cm ⁻²)	135.8	1.409	[¹⁰⁰]
N/P-C-CoP-850	773.8 (5 mA cm ⁻²)	151	1.46	[¹⁰¹]
FeCoP/NPC	784 (2 mA cm ⁻²)	74	1.51	[¹⁰²]
CoPx@CNS	110	1.4	[¹⁰³]
Co₂P/CoNPC	116	1.42	[⁷⁶]
CoO/Co_xP	122.73	0.74	1.4	[¹⁰⁴]
CoP@PNC-DoS	730.55	138.6	0.78	1.41	55 ₃₀	[⁷⁸]
Co₉S₈/P@CS	142.50	1.34	[¹⁰⁵]
FeNiP/NPCS	602.7 (10 mA cm ⁻²)	163	783.5 (10 mA cm ⁻²)	0.8	1.51	69 ₁₀	[¹⁰⁶]
CoP/NP-HPC	186	1.4	[¹⁰⁷]
BPCC-0.25 (CoP)	785.8 (5 mA cm ⁻²)	120	1.41	[¹⁰⁸]
CoP-PBSCF	138	58.3 ₁₀	[¹⁰⁹]
FeNiP/NCH	250	0.73	1.48	[¹¹⁰]
Co/CoxMy	125.2	1.425	61 ₁₀	[⁹³]

Mn _x (PO ₄) _y /NPC	668 (20 mA cm ⁻²)	[⁹⁴]
CoP NCs	61	1.34	[⁹⁵]
Co ₂ P/CoN-in-NCNTs	844.5	194.6	0.8	1.36	[¹¹¹]
Mesoporous Co₃O₄	542 (2 A cm ⁻²)	546 (2 A cm ⁻²)	1.32	[¹¹²]
NCMP	740.3 (5 A cm ⁻²)	148	932 (5 mA cm ⁻²)	0.68	1.42	75 ₅	This Work	

Table S3: Comparison of $E_{1/2}$ and E_{Onset} for the Pt/C/GC, NCMP/GC, NCMP1/GC, and NCP/GC Electrodes

Catalyst	$E_{1/2}$ (V)	E_{onset} (V)
Pt/C/GC	0.82	0.91
NCMP/GC	0.76	0.85
NCMP1/GC	0.74	0.83
NCP/GC	0.73	0.80

Table S4: Comparison of the Number of Electrons Per Oxygen Molecule (n) for the Pt/C/GC, NCMP/GC, NCMP1/GC, and NCP /GC Electrodes

Catalyst	n
Pt/C/GC	3.97 (@ ~790 mV)
NCMP/GC	3.97 (@ 755 mV)
NCMP1/GC	2.9 (@ 700 mV)
NCP/GC	2.05 (@ 700 mV)

References

1. A. J. Bard, L. R. Faulkner and H. S. White, *Electrochemical Methods: Fundamentals and Applications*, 3rd ed., John Wiley & Sons, USA 2022.
2. H. Liang, A. N. Gandi, D. H. Anjum, X. Wang, U. Schwingenschlögl and H. N. Alshareef, *Nano Lett.*, 2016, **16**, 7718-7725.
3. Z.-Q. Liu, H. Cheng, N. Li, T. Y. Ma and Y.-Z. Su, *Adv. Mater.*, 2016, **28**, 3777-3784.
4. I. S. Amiinu, Z. Pu, X. Liu, K. A. Owusu, H. G. R. Monestel, F. O. Boakye, H. Zhang and S. Mu, *Adv. Funct. Mater.*, 2017, **27**, 1702300.
5. K. Wu, L. Zhang, Y. Yuan, L. Zhong, Z. Chen, X. Chi, H. Lu, Z. Chen, R. Zou, T. Li, C. Jiang, Y. Chen, X. Peng and J. Lu, *Adv. Mater.*, 2020, **32**, 2002292.
6. T. Zhou, H. Shan, H. Yu, C. a. Zhong, J. Ge, N. Zhang, W. Chu, W. Yan, Q. Xu, H. a. Wu, C. Wu and Y. Xie, *Adv. Mater.*, 2020, **32**, 2003251.
7. L. Yan, Y. Xu, P. Chen, S. Zhang, H. Jiang, L. Yang, Y. Wang, L. Zhang, J. Shen and X. Zhao, *Adv. Mater.*, 2020, **32**, 2003313.
8. M. Jiang, H. Zhai, L. Chen, L. Mei, P. Tan, K. Yang and J. Pan, *Adv. Funct. Mater.*, 2023, **33**, 2302621.
9. A. Gupta, C. A. Allison, A. Kumar, R. Srivastava, W. Lin, J. Sultana, S. R. Mishra, F. Perez, R. K. Gupta and T. Dawsey, *J. Energy Storage*, 2023, **73**, 108824.
10. Y. Deng, Y. Cao, Y. Xia, X. Xi, Y. Wang, W. Jiang, D. Yang, A. Dong and T. Li, *Adv. Energy Mater.*, 2022, **12**, 2202394.
11. E. Vijayakumar, S. Ramakrishnan, C. Sathiskumar, D. J. Yoo, J. Balamurugan, H. S. Noh, D. Kwon, Y. H. Kim and H. Lee, *Chem. Eng. J.*, 2022, **428**, 131115.
12. X. Guo, M. Li, L. Qiu, F. Tian, L. He, S. Geng, Y. Liu, Y. Song, W. Yang and Y. Yu, *Chem. Eng. J.*, 2023, **453**, 139796.
13. J. Zhu, E. Jiang, X. Wang, Z. Pan, X. Xu, S. Ma, P. Kang Shen, L. Pan, M. Eguchi, A. K. Nanjundan, J. Shapter and Y. Yamauchi, *Chem. Eng. J.*, 2022, **427**, 130946.
14. K. Zheng, J. Ren, X. Li, G. Li, L. Jiao and C. Xu, *Chem. Eng. J.*, 2022, **441**, 136031.
15. Y. Zhao, N. Dongfang, C. A. Triana, C. Huang, R. Erni, W. Wan, J. Li, D. Stoian, L. Pan, P. Zhang, J. Lan, M. Iannuzzi and G. R. Patzke, *Energy Environ. Sci.*, 2022, **15**, 727-739.
16. W. Zhang, N. Han, J. Luo, X. Han, S. Feng, W. Guo, S. Xie, Z. Zhou, P. Subramanian, K. Wan, J. Arbiol, C. Zhang, S. Liu, M. Xu, X. Zhang and J. Fransaer, *Small*, 2022, **18**, 2103561.
17. C. Zhang, Y. Han, W. Wang, R. Huang, R. Ma and J. Yan, *ACS Appl. Energy Mater.*, 2022, **5**, 9392-9401.
18. H. Xiang, W. Chen, T. Li, J. Huang, G. Chen, T. Gong and K. Ken Ostrikov, *Chem. Eng. J.*, 2022, **446**, 137419.
19. J. Wu, Z.-F. Wang, T. Guan, G. Zhang, J. Zhang, J. Han, S. Guan, N. Wang, J. Wang and K. Li, *Carbon Energy*, 2023, **5**, e268.
20. P. Wang, Y. Luo, G. Zhang, M. Wu, Z. Chen, S. Sun and Z. Shi, *Small*, 2022, **18**, 2105803.
21. L. Wang, Y. Zhao, Z. Huang, X. Rao, M. Guo, T. T. Isimjan and X. Yang, *ChemCatChem*, 2022, **14**, e202101933.
22. Y. Tan, J. Feng, L. Kang, L. Liu, F. Zhao, S. Zhao, D. J. L. Brett, P. R. Shearing, G. He and I. P. Parkin, *Energy Environ. Mater.*, 2022, **6**, e12398.
23. Y. Sun, T. Liu, Z. Li, A. Meng, G. Li, L. Wang and S. Li, *Chem. Eng. J.*, 2022, **433**, 133684.
24. M. Sun, R. Ge, J. Yang, J. Qu, Y. Li, M. Zhu, J. M. Cairney, R. Zheng, S. Li and W. Li, *Applied Energy*, 2022, **326**, 119999.
25. H. Song, J. Yu, Z. Tang, B. Yang and S. Lu, *Adv. Energy Mater.*, 2022, **12**, 2102573.
26. K. E. Salem, A. A. Saleh, G. E. Khedr, B. S. Shaheen and N. K. Allam, *Energy Environ. Mater.*, 2023, **6**, e12324.
27. Q. Quan, Y. Zhang, F. Wang, X. Bu, W. Wang, Y. Meng, P. Xie, D. Chen, W. Wang, D. Li, C. Liu, S. Yip and J. C. Ho, *Nano Energy*, 2022, **101**, 107566.
28. T. X. Nguyen, N. H. Ting and J. M. Ting, *J. Power Sources*, 2022, **552**, 232249.

29. D. N. Nguyen, T. K. C. Phu, J. Kim, W. T. Hong, J. S. Kim, S. H. Roh, H. S. Park, C. H. Chung, W. S. Choe, H. Shin, J. Y. Lee and J. K. Kim, *Small*, 2022, **18**, 2204797.
30. H. Liu, S. Yang, J. Ma, M. Dou and F. Wang, *Nano Energy*, 2022, **98**, 107315.
31. H. Liu, J. Gao, X. Xu, Q. Jia, L. Yang, S. Wang and D. Cao, *Chem. Eng. J.*, 2022, **448**, 137706.
32. W. Li, G. Cheng, S. Peng, M. Sun, S. Wang, S. Han, Y. Liu, T. Zhai and L. Yu, *Chem. Eng. J.*, 2022, **430**, 132699.
33. S. Li, L. Wang, H. Su, A. N. Hong, Y. Wang, H. Yang, L. Ge, W. Song, J. Liu, T. Ma, X. Bu and P. Feng, *Adv. Funct. Mater.*, 2022, **32**, 2200733.
34. J. Hu, Y. Qin, H. Sun, Y. Ma, L. Lin, Y. Peng, J. Zhong, M. Chen, X. Zhao and Z. Deng, *Small*, 2022, **18**, 2106260.
35. J. Ge, Y. Chen, Y. Zhao, Y. Wang, F. Zhang and X. Lei, *ACS Appl. Mater. Interfaces*, 2022, **14**, 26846-26857.
36. J. Gao, X. Yu, Y. Li and Y. Ma, *ChemCatChem*, 2022, **14**, e202200558.
37. H. Cui, M. Jiang, G. Tan, J. Xie, P. Tan and J. Pan, *ChemElectroChem*, 2022, **9**, e202101482.
38. J. Cheng, B. Shen, Y. Song, J. Liu, Q. Ye, M. Mao and Y. Cheng, *Chem. Eng. J.*, 2022, **428**, 131130.
39. M. Chen, H. Li, C. Wu, Y. Liang, J. Qi, J. Li, E. Shangguan, W. Zhang and R. Cao, *Adv. Funct. Mater.*, 2022, **32**, 2206407.
40. S. Bera, H. J. Woo, H. Khan, S. Y. Park, J. H. Baek, W. J. Lee and S. H. Kwon, *Chem. Eng. J.*, 2022, **448**, 137716.
41. T. N. Batugedara and S. L. Brock, *Chem. Mater.*, 2022, **34**, 4414-4427.
42. Y. Zhu, L. Zhang, X. Zhang, Z. Li, M. Zha, M. Li and G. Hu, *Chem. Eng. J.*, 2021, **405**, 127002.
43. J. Zhou, Y. Dou, T. He, X. J. Kong, L. H. Xie and J. R. Li, *J. Energy Chem.*, 2021, **63**, 253-261.
44. J. Zhang, H. Zhou, Y. Liu, J. Zhang, Y. Cui, J. Li, J. Lian, G. Wang and Q. Jiang, *ACS Appl. Mater. Interfaces*, 2021, **13**, 52598-52609.
45. S. F. Zai, Y. T. Zhou, C. C. Yang and Q. Jiang, *Chem. Eng. J.*, 2021, **421**, 127856.
46. F. Yang, T. Xiong, P. Huang, S. Zhou, Q. Tan, H. Yang, Y. Huang and M. S. J. T. Balogun, *Chem. Eng. J.*, 2021, **423**, 130279.
47. D. Yang, Z. Su, Y. Chen, K. Srinivas, J. Gao, W. Zhang, Z. Wang and H. Lin, *Small*, 2021, **17**, 2006881.
48. D. Yang, W. Hou, Y. Lu, W. Zhang and Y. Chen, *J. Energy Chem.*, 2021, **52**, 130-138.
49. X. Xu, T. Wang, L. Su, Y. Zhang, L. Dong and X. Miao, *ACS Sustain. Chem. Eng.*, 2021, **9**, 5693-5704.
50. X. Xu, A. Cao, W. You, Z. Tao, L. Kang and J. Liu, *Small*, 2021, **17**, 2101725.
51. X. Wu, R. Wang, W. Li, B. Feng and W. Hu, *ACS Appl. Nano Mater.*, 2021, **4**, 3369-3376.
52. L. Wu, L. Yu, F. Zhang, B. McElhenney, D. Luo, A. Karim, S. Chen and Z. Ren, *Adv. Funct. Mater.*, 2021, **31**, 2006484.
53. P. Wei, X. Sun, M. Wang, J. Xu, Z. He, X. Li, F. Cheng, Y. Xu, Q. Li, J. Han, H. Yang and Y. Huang, *ACS Appl. Mater. Interfaces*, 2021, **13**, 53955-53964.
54. Y. N. Wang, Z. J. Yang, D. H. Yang, L. Zhao, X. R. Shi, G. Yang and B. H. Han, *ACS Appl. Mater. Interfaces*, 2021, **13**, 8832-8843.
55. X. Wang, C. Wang, F. Lai, H. Sun, N. Yu and B. Geng, *ACS Appl. Nano Mater.*, 2021, **4**, 12083-12090.
56. S. Wang, J. Cai, C. Lv, C. Hu, H. Guan, J. Wang, Y. Shi, J. Song, A. Watanabe and X. Ge, *Chem. Eng. J.*, 2021, **420**, 129972.
57. L. Wang, J. Fan, Y. Liu, M. Chen, Y. Lin, H. Bi, B. Liu, N. Shi, D. Xu, J. Bao and M. Han, *Adv. Funct. Mater.*, 2021, **31**, 2010912.
58. Y. Tian, S. Li, P. Qin, Q. Wang, P. Liu, X. Ji and Q. Jing, *ChemCatChem*, 2021, **13**, 3037-3045.
59. U. P. Suryawanshi, U. V. Ghorpade, D. M. Lee, M. He, S. W. Shin, P. V. Kumar, J. S. Jang, H. R. Jung, M. P. Suryawanshi and J. H. Kim, *Chem. Mater.*, 2021, **33**, 234-245.
60. H. Song, M. Wu, Z. Tang, J. S. Tse, B. Yang and S. Lu, *Angew. Chem. Int. Ed.*, 2021, **60**, 7234-7244.

61. J. Shi, F. Qiu, W. Yuan, M. Guo and Z. H. Lu, *Chem. Eng. J.*, 2021, **403**, 126312.
62. S. Riyajuddin, K. Azmi, M. Pahuja, S. Kumar, T. Maruyama, C. Bera and K. Ghosh, *ACS Nano*, 2021, **15**, 5586-5599.
63. Q. Quan, Z. Lai, Y. Bao, X. Bu, Y. Meng, W. Wang, T. Takahashi, T. Hosomi, K. Nagashima, T. Yanagida, C. Liu, J. Lu and J. C. Ho, *Small*, 2021, **17**, 2006860.
64. S. M. Pawar, A. T. Aqueel Ahmed, C. H. Lee, P. T. Babar, J. H. Kim, S. U. Lee, H. Kim and H. Im, *ACS Appl. Energy Mater.*, 2021, **4**, 14169-14179.
65. Z. Lv, W. Ma, M. Wang, J. Dang, K. Jian, D. Liu and D. Huang, *Adv. Funct. Mater.*, 2021, **31**, 2102576.
66. X. W. Lv, W. S. Xu, W. W. Tian, H. Y. Wang and Z. Y. Yuan, *Small*, 2021, **17**, 2101856.
67. B. Lu, J. Zang, W. Li, J. Li, Q. Zou, Y. Zhou and Y. Wang, *Chem. Eng. J.*, 2021, **422**, 130062.
68. S. Liu, Z. Lin, R. Wan, Y. Liu, Z. Liu, S. Zhang, X. Zhang, Z. Tang, X. Lu and Y. Tian, *J. Mater. Chem. A*, 2021, **9**, 21259-21269.
69. H. Liu, Z. Liu, Y. Wang, J. Zhang, Z. Yang, H. Hu, Q. Zhao, H. Ning, L. Zhi and M. Wu, *Carbon*, 2021, **182**, 327-334.
70. W. Li, Y. Jiang, Y. Li, Q. Gao, W. Shen, Y. Jiang, R. He and M. Li, *Chem. Eng. J.*, 2021, **425**, 130651.
71. N. Li, Y. Guan, Y. Li, H. Mi, L. Deng, L. Sun, Q. Zhang, C. He and X. Ren, *J. Mater. Chem. A*, 2021, **9**, 1143-1149.
72. L. Li, W. Zou, Q. Ye, Q. Li, Q. Feng, J. Wei, X. Xu and F. Wang, *J. Power Sources*, 2021, **516**, 230657.
73. J. Li, H. Huang, X. Cao, H. H. Wu, K. Pan, Q. Zhang, N. Wu and X. Liu, *Chem. Eng. J.*, 2021, **416**, 127677.
74. D. Lai, Q. Kang, F. Gao and Q. Lu, *J. Mater. Chem. A*, 2021, **9**, 17913-17922.
75. D. Kim, X. Qin, B. Yan and Y. Piao, *Chem. Eng. J.*, 2021, **408**, 127331.
76. H. Liu, J. Guan, S. Yang, Y. Yu, R. Shao, Z. Zhang, M. Dou, F. Wang and Q. Xu, *Adv. Mater.*, 2020, **32**, e2003649.
77. X. Li, L. Xiao, L. Zhou, Q. Xu, J. Weng, J. Xu and B. Liu, *Angew. Chem. Int. Ed.*, 2020, **59**, 21106-21113.
78. Y. Li, Y. Liu, Q. Qian, G. Wang and G. Zhang, *Energy Storage Mater.*, 2020, **28**, 27-36.
79. H. Feng, L. Tang, G. Zeng, J. Yu, Y. Deng, Y. Zhou, J. Wang, C. Feng, T. Luo and B. Shao, *Nano Energy*, 2020, **67**, 104174.
80. L. Chai, Z. Hu, X. Wang, Y. Xu, L. Zhang, T. T. Li, Y. Hu, J. Qian and S. Huang, *Adv. Sci.*, 2020, **7**, 1903195.
81. L. Ji, J. Wang, X. Teng, T. J. Meyer and Z. Chen, *ACS Catal.*, 2020, **10**, 412-419.
82. L. Yan, B. Zhang, S. Wu and J. Yu, *J. Mater. Chem. A*, 2020, **8**, 14234-14242.
83. X. Luo, P. Ji, P. Wang, R. Cheng, D. Chen, C. Lin, J. Zhang, J. He, Z. Shi, N. Li, S. Xiao and S. Mu, *Adv. Energy Mater.*, 2020, **10**, 1903891.
84. C. Lin, D. Wang, H. Jin, P. Wang, D. Chen, B. Liu and S. Mu, *J. Mater. Chem. A*, 2020, **8**, 4570-4578.
85. D. Chen, Z. Pu, R. Lu, P. Ji, P. Wang, J. Zhu, C. Lin, H. W. Li, X. Zhou, Z. Hu, F. Xia, J. Wu and S. Mu, *Adv. Energy Mater.*, 2020, **10**, 2000814.
86. A. Baby, D. Singh, C. Murugesan and P. Barpanda, *Chem. Commun.*, 2020, **56**, 8400-8403.
87. H. Yan, Y. Xie, A. Wu, Z. Cai, L. Wang, C. Tian, X. Zhang and H. Fu, *Adv. Mater.*, 2019, **31**, 1901174.
88. H. Sun, Y. Min, W. Yang, Y. Lian, L. Lin, K. Feng, Z. Deng, M. Chen, J. Zhong, L. Xu and Y. Peng, *ACS Catal.*, 2019, **9**, 8882-8892.
89. F. Bu, W. Chen, M. F. Aly Aboud, I. Shakir, J. Gu and Y. Xu, *J. Mater. Chem. A*, 2019, **7**, 14526-14535.
90. L. Yan, B. Zhang, J. Zhu, S. Zhao, Y. Li, B. Zhang, J. Jiang, X. Ji, H. Zhang and P. K. Shen, *J. Mater. Chem. A*, 2019, **7**, 14271-14279.
91. L. Yan, B. Zhang, J. Zhu, Z. Liu, H. Zhang and Y. Li, *J. Mater. Chem. A*, 2019, **7**, 22453-22462.

92. B. Weng, X. Wang, C. R. Grice, F. Xu and Y. Yan, *J. Mater. Chem. A*, 2019, **7**, 7168-7178.
93. J. Chen, C. Fan, X. Hu, C. Wang, Z. Huang, G. Fu, J. M. Lee and Y. Tang, *Small*, 2019, **15**, 1901518.
94. S. Wang, G. Nam, P. Li, H. Jang, J. Wang, M. G. Kim, Z. Wu, X. Liu and J. Cho, *ChemCatChem*, 2019, **11**, 1222-1227.
95. H. Li, Q. Li, P. Wen, T. B. Williams, S. Adhikari, C. Dun, C. Lu, D. Itanze, L. Jiang, D. L. Carroll, G. L. Donati, P. M. Lundin, Y. Qiu and S. M. Geyer, *Adv. Mater.*, 2018, **30**, 1705796.
96. H. Zhang, X. Li, A. Hähnle, V. Naumann, C. Lin, S. Azimi, S. L. Schweizer, A. W. Maijenburg and R. B. Wehrspohn, *Adv. Funct. Mater.*, 2018, **28**, 1706847.
97. L. Yan, L. Cao, P. Dai, X. Gu, D. Liu, L. Li, Y. Wang and X. Zhao, *Adv. Funct. Mater.*, 2017, **27**, 1703455.
98. Y. Tan, H. Wang, P. Liu, Y. Shen, C. Cheng, A. Hirata, T. Fujita, Z. Tang and M. Chen, *Energy Environ. Sci.*, 2016, **9**, 2257-2261.
99. D. Li, H. Baydoun, C. N. Verani and S. L. Brock, *J. Am. Chem. Soc.*, 2016, **138**, 4006-4009.
100. H. W. Go, T. T. Nguyen, Q. P. Ngo, R. Chu, N. H. Kim and J. H. Lee, *Small*, 2023, **19**, 2206341.
101. L. Lin, H. Sun, X. Yuan, Y. Gu, Q. Mu, P. Qi, T. Yan, L. Zhang, Y. Peng and Z. Deng, *Chem. Eng. J.*, 2022, **428**, 131225.
102. H. Chen, Y. Liu, B. Liu, M. Yang, H. Li and H. Chen, *Nanoscale*, 2022, **14**, 12431-12436.
103. C. C. Hou, L. Zou, Y. Wang and Q. Xu, *Angew. Chem. Int. Ed.*, 202010.1002/anie.202011347.
104. Y. Niu, M. Xiao, J. Zhu, T. Zeng, J. Li, W. Zhang, D. Su, A. Yu and Z. Chen, *J. Mater. Chem. A*, 2020, **8**, 9177-9184.
105. W. Li, Y. Li, H. Fu, G. Yang, Q. Zhang, S. Chen and F. Peng, *Chem. Eng. J.*, 2020, **381**, 122683.
106. J. T. Ren, Y. S. Wang, L. Chen, L. J. Gao, W. W. Tian and Z. Y. Yuan, *Chem. Eng. J.*, 2020, **389**, 124408.
107. Y. Wang, M. Wu, J. Li, H. Huang and J. Qiao, *J. Mater. Chem. A*, 2020, **8**, 19043-19049.
108. J. Hu, X. Yuan, C. Wang, X. Shao, B. Yang, A. Abdul Razzaq, X. Zhao, Y. Lian, Z. Deng, M. Chen and Y. Peng, *Small*, 2020, **16**, 2000755.
109. Y. Q. Zhang, H. B. Tao, Z. Chen, M. Li, Y. F. Sun, B. Hua and J. L. Luo, *J. Mater. Chem. A*, 2019, **7**, 26607-26617.
110. Y. S. Wei, M. Zhang, M. Kitta, Z. Liu, S. Horike and Q. Xu, *J. Am. Chem. Soc.*, 2019, **141**, 7906-7916.
111. Y. Guo, P. Yuan, J. Zhang, H. Xia, F. Cheng, M. Zhou, J. Li, Y. Qiao, S. Mu and Q. Xu, *Adv. Funct. Mater.*, 2018, **28**, 1805641.
112. X. Chen, B. Liu, C. Zhong, Z. Liu, J. Liu, L. Ma, Y. Deng, X. Han, T. Wu, W. Hu and J. Lu, *Adv. Energy Mater.*, 2017, **7**, 1700779.